



# ADAPTIVE BACKSTEPPING CONTROLLER DESIGN AND IMPLEMENTATION FOR A MATRIX-CONVERTER-BASED IM DRIVE SYSTEM

R.R. Joshi, R.A. Gupta and A.K. Wadhvani

R. R. Joshi is with Department of Electrical Engineering, CTAE, Udaipur (Raj.), India;

R. A. Gupta is with Department of Electrical Engineering, MNIT, Jaipur, (Raj.), India;

A. K. Wadhvani is with Department of Electrical Engineering, MITS, Gwalior (MP), India

## ABSTRACT

A systematic controller design and implementation for a matrix-converter-based induction motor drive system is proposed. A nonlinear adaptive backstepping controller is proposed to improve the speed and position responses of the induction motor system. By using the proposed adaptive backstepping controller, the system can track a time-varying speed command and a time-varying position command well. Moreover, the system has a good load disturbance rejection capability. The realisation of the controller is very simple. All of the control loops, including the current loop, speed loop and position loop, are implemented by a digital signal processor. Several experimental results are given to validate the theoretical analysis.

## 1 INTRODUCTION

An AC/AC converter is used to provide sinusoidal output voltages with varying amplitudes and frequencies, and to draw sinusoidal input currents from the AC source. The rectifier / DC-link / inverter is widely used in conventional AC drive systems. The DC-link requires a large capacitor as an energy storage component. The capacitor can be a critical component because it is large and expensive. The power factor and current harmonics of the input AC side are not good enough. In addition, a braking resistance is required to absorb the energy during braking the drive system. In AC/AC converter applications, the matrix converter has become increasingly attractive in recent years.

The AC/AC matrix converter has several advantages. For example, the matrix converter is a single-stage converter. It does not require any DC-link energy storage component. In addition, it has a high-power-factor sinusoidal input current with a bidirectional power flow for the whole matrix converter drive system. In the past, the matrix converter, therefore, was developed in the research laboratory only and could not be popularly used in industry. The situation has been changed. Recently, Eupec Co. has developed a new technology for integrating the whole matrix-converter power device in a single package. In addition, the integrated power modules are now available

commercially. This type of packaging can minimise the stray inductance and the size of the power devices [1]. Yaskawa Co. has implemented a commercial matrix converter and has shown it has many advantages. Currently, the cost of the matrix converter is a little higher than the rectifier/DClink/ inverter. However, in the future, after the matrix converter becomes more and more popular, the cost of the matrix converter will be reduced and will compete with the traditional rectifier/DC-link/ inverter [2].

The matrix converter is superior to the traditional PWM (Pulse width modulation) drives because of regeneration ability and sinusoidal input current [3-5]. Therefore it meets the stringent energy-efficiency and power quality requirements of the new century. Matrix converter can be considered to be a direct converter, in this respect similar to a cycloconverter, because, first, it doesn't employ a dc link and, secondly the output waveforms are composed of switched segments of the input waveforms. The matrix converter therefore possesses the advantages of both the cycloconverter and the PWM drive, as summarized below :

1. It can operate in all four quadrants of the torque-speed plane because of its regeneration capability.
2. Its input current waveform is sinusoidal and the input power factor is unity



3. The input power factor may be controlled across the whole speed range.
4. There is no dc link and therefore no requirement for energy storage devices
5. The output voltage and input current waveforms can be controlled such that they are near sinusoidal in form.
6. The harmonic distortion that is incurred is at high frequencies
7. It may be used as direct frequency changer, converting a fixed ac or dc source into a variable ac or dc supply.
8. Compact converter design.
9. No dc-link components.

Several publications on matrix converters have dealt with modulation strategies to improve the performance of the matrix converter [6–8]. Some papers discussed the protection issues of the matrix converter [9]. Unfortunately, only very few publications have considered the controller design and position control methods for the matrix-converter-based AC drive system [10]. Owing to its possible popularity in the future of the matrix converter drive system, the controller design is very challenging. The major reason is that the switching frequency of a matrix converter is lower compared to that of the rectifier/DC-link/inverter. As a result, the matrix converter produces larger current harmonics and torque pulsations than the AC motor, which causes serious uncertainty in the dynamic model and makes the controller design more difficult. As a result, it is very challenging to achieve a high-performance speed or position drive system by using a matrix converter.

With respect to controller design, a proportional–integral (PI) controller has been widely used in many industrial drives because of its simple and reliable characteristics. However, this PI controller cannot obtain both a good command tracking ability and a rapid recovery of the external load disturbance. To resolve this problem, a two degree-of-freedom controller was designed [11]. By using the two-degree-of-freedom controller, the transient response and load disturbance rejection response can be individually controlled. As a result, better performance can be obtained for a step input command and load disturbance. Unfortunately, when a time-varying command is applied, the linear control system produces a steady-state amplitude error and phase delay in output responses.

To improve the tracking ability of the time-varying command, this paper proposes a nonlinear adaptive backstepping control algorithm for a matrix-converter-based IM drive system. Although the theoretical development of the nonlinear adaptive backstepping control algorithm has been well developed in [12], there are only a few applications in motor drives [13]. This paper, therefore, applies the nonlinear backstepping controller for a matrix-converter-based IM drive system. According to the experimental results, the transient responses, load disturbance responses and tracking responses of the speed- and position-control IM drive systems are effectively improved.

In this paper, a novel matrix-converter-based IM control system is proposed. All of the current, speed and position loops are implemented by a digital signal processor. After the adaptive backstepping speed- and position control algorithms are applied, a satisfactory control performance can be achieved. In addition, the system can track both speed and position time-varying commands well. To the authors' best knowledge, this is the first time that the adaptive backstepping controller has been applied in a high-performance matrix-converter-based IM system. Moreover, the implementation of the control law is very simple by using a digital signal processor and can be applied for both speed and position-control systems.

## 2 SYSTEM DESCRIPTION

### 2.1 Matrix Converter Drive System

The block diagram to be considered in this paper is shown in Fig. 1a. The hardware of the system consists of a three-phase IM and load, a nine-switch matrix converter, and a digital signal processor system. The motor chosen for the study is a three-phase, Y-connected, IM. Its rated speed is 1500 rpm. A resolver is mounted on the motor shaft for velocity and position sensing. Two Hall effect current sensors are used to detect the stator currents of the motor because the drive system is a three-phase balanced system. The drive system works as follows. First, the position (speed) command is compared with the feedback position (speed). Next, the position (speed) controller generates the q-axis current command and then transfers into three-phase current commands. After that, the three-phase current commands are compared with the three-phase

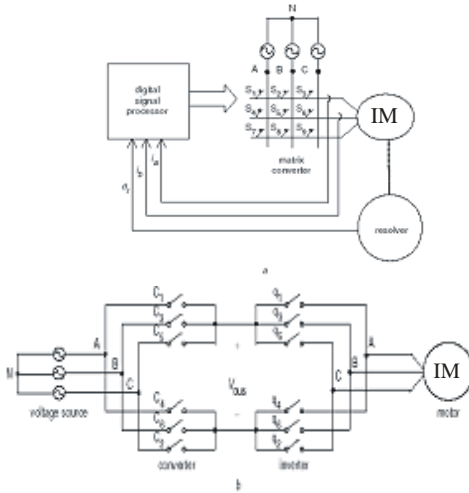


**Fig. 1.** Drive system configuration (a) Block diagram of whole drive (b) Virtual equivalent circuit

feedback currents, which thus determines the switching states of the matrix converter. The details of the switching algorithm of the matrix converter are discussed in the following Section. Finally, the motor rotates, and a closed-loop drive system is thus achieved.

### 2.2 Switching Algorithm of Matrix Converter

The switching patterns of the nine switches of the matrix converter should satisfy the basic requirements. For instance, the switches of the matrix converter cannot short circuit the input voltage sources. In addition, the switches of the matrix converter cannot open the output load currents because the load is an inductive load. Generally speaking, there are two major switching methods for the matrix converter: direct and indirect. The direct method provides the output currents or voltages by using only six switching patterns. By suitably controlling the duty cycle of the nine switches under the six switching patterns, the required output voltage can be obtained. This method, however, requires a lot of computations to determine the switching states. The indirect switching method is based on the basic principle of the switching strategy of the conventional converter and inverter. The switching algorithm of the indirect switching method can be explained using a virtual equivalent circuit. The virtual equivalent circuit, shown in Fig. 1b, consists of an AC/DC converter and a DC/AC inverter. In addition, the AC/DC converter and DC/AC inverter are controlled independently.

The virtual DC-bus voltage is obtained by selecting the switches of the AC/DC converter. In addition, the virtual DC-bus voltage can be suitably adjusted if one selects different switching states of the AC/DC converter. The virtual DC/AC inverter is used to regulate the three-phase output currents. Take the A-phase as an example. When the A-phase current command is larger than the A-phase current, the upper switch of the A-phase leg is turned on. As a result, the A-phase current increases to track the current command. On the other hand, when the A-phase current command is smaller than the A-phase current, the lower switch of the A-phase leg is turned on. Then, the A-phase current decreases to track the current command. The B-phase and C-phase current regulators are operated using the same method. Finally, by mapping the switching states of the AC/DC converter and the DC/AC inverter into the real matrix converter, one can determine the switching condition of the matrix converter [14, 15].

### 3 CONTROLLER DESIGN

The adaptive backstepping controller is designed for speed control and position control. In this Section, first, the mathematical model of the uncontrolled plant is discussed. Next, the nonlinear speed controller is discussed. Finally, the nonlinear position controller is presented.

#### 3.1 Mathematical Model of Uncontrolled Plant

The uncontrolled model of a IM with a current regulated inverter can be described by the following differential equations [12]:

$$\dot{\omega}_r = -\frac{B}{J}\omega_r + \frac{k_t}{J}(u + d) \quad (1)$$

$$\dot{\theta}_r = \omega_r \quad (2)$$

where  $J$  is the motor shaft inertia,  $B$  is the motor viscous coefficient,  $k_t$  is the torque constant,  $u$  is the control input,  $d$  is the total value of equivalent load disturbance and system parameter uncertainties,  $\omega_r$  is the speed of the motor, and  $\theta_r$  is the angle of the motor.

#### 3.2 Nonlinear Speed Controller Design

The block diagram of the speed control system is shown in Fig. 2. To design an adaptive backstepping speed controller, the speed tracking error can be defined as

$$e_1 = \omega_r - \omega_r^* \quad (3)$$

Now, take the derivative of both sides to obtain



$$\dot{e}_1 = \dot{\omega}_r - \dot{\omega}_r^* \quad (4)$$

Define the stability function as

$$\alpha_{\omega 1} = -c_{\omega 1} e_1 + \dot{\omega}_r^* \quad (5)$$

where  $C_{w1}$  is a positive constant, and  $\alpha_{w1}$  is the stability function. The Lyapunov function can be selected as

$$V_{\omega 1} = \frac{1}{2} e_1^2 \quad (6)$$

Furthermore, define  $e_2$  and, substituting (1) into it, we can obtain

$$e_2 = \dot{\omega}_r - \alpha_{\omega 1} = -\frac{B}{J} \omega_r + \frac{k_t}{J} (u + d) - \alpha_{\omega 1} \quad (7)$$

Then, by taking the differential of  $V_{w1}$  and substituting (4), (5), and (7) into it, we can obtain

$$\dot{V}_{\omega 1} = e_1 e_2 - c_{\omega 1} e_1^2 \quad (8)$$

To design the controller, which has the ability to track commands and to reject load disturbance, we add the related terms of  $d$  into  $V_{w1}$  to obtain a new Lyapunov function as [12]

$$V_{\omega 2} = V_{\omega 1} + \frac{1}{2} \frac{1}{\gamma_{\omega}} \tilde{d}^2 \quad (9)$$

where  $\tilde{d}$  is the error between the value of  $d$  and its estimated value  $\hat{d}$ , and  $\gamma_{\omega}$  is a positive constant. After that, by taking the differential of  $V_{\omega 2}$  and substituting (7) and (8) into the differential result, it is not difficult to obtain

$$\begin{aligned} \dot{V}_{\omega 2} &= \dot{V}_{\omega 1} + \frac{1}{\gamma_{\omega}} \tilde{d} \dot{\tilde{d}} \\ &= -c_{\omega 1} e_1^2 + e_1 \left[ -\frac{B}{J} \omega_r + \frac{k_t}{J} (u + \hat{d}) - \alpha_{\omega 1} \right] \\ &\quad - \frac{1}{\gamma_{\omega}} \tilde{d} (\dot{\tilde{d}} - \gamma_{\omega} e_1) \end{aligned} \quad (10)$$

According to (10), the control input  $u$  can be designed as

$$u = \frac{J}{k_t} \left( -c_{\omega 2} e_1 + \alpha_{\omega 1} - \frac{k_t}{J} \hat{d} + \frac{B}{J} \omega_r \right) \quad (11)$$

where  $c_{\omega 2}$  is a positive constant. Then, the estimated value,  $\hat{d}$ , can be obtained by solving the following:

$$\dot{\hat{d}} = \gamma_{\omega} e_1 \quad (12)$$

Substituting (11) and (12) into (10),  $V_{\omega 2}$  can be determined as

$$\dot{V}_{\omega 2} = -(c_{\omega 1} + c_{\omega 2}) e_1^2 \leq 0 \quad (13)$$

From (13), one can obtain that the Lyapunov function is a non-increasing function because its derivative is equal to or less than zero. By integrating both sides of (13), one can obtain

$$\begin{aligned} \int_0^{\infty} \dot{V}_{\omega 2}(\tau) d\tau &= V_{\omega 2}(e_1(\infty), \tilde{d}_1(\infty)) \\ &\quad - V_{\omega 2}(e_1(0), \tilde{d}_1(0)) \end{aligned}$$

The values of  $e_1(0)$ ,  $\tilde{d}_1(0)$  are bounded. In addition,  $\dot{V}_{\omega 2} \leq 0$ , therefore  $e_1(\infty)$  are also bounded. We can observe that the integration of  $\dot{V}_{\omega 2}$  is bounded. It is easy to understand that the integration of the  $e_1^2$  is bounded as well. After deriving that  $e_1(t)$  is uniformly continuous, one can use Bardalal's lemma and obtain the following :

$$\lim_{t \rightarrow \infty} e_1(t) = 0 \quad (15)$$

To design the controller, which has the ability to track commands and to reject load disturbance, we add the related terms of  $\tilde{d}$  into  $V_{\omega 1}$  to obtain a new Lyapunov function as [12]

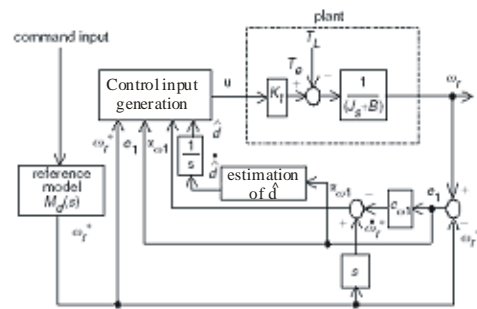


Fig. 2.

### 3.3 Nonlinear Position Controller Design

The position tracking error of the position control system can be defined as

$$z_1 = \theta_r - \theta_r^* \quad (16)$$

Now, by taking the derivative of both sides, one can obtain

$$\dot{z}_1 = \omega_r - \dot{\theta}_r^* \quad (17)$$

Define a stability function as

$$\alpha_{\theta 1} = -c_{\theta 1} z_1 + \dot{\theta}_r^* \quad (18)$$



where  $C_2$  is positive, and  $a_{y1}$  is a stability function. The Lyapunov function is selected as [12]

$$V_{\theta 1} = \frac{1}{2} z_1^2 \quad (19)$$

Furthermore, defined  $Z_2$  as

$$z_2 = \omega_r - \alpha_{\theta 1} \quad (20)$$

Then, taking the differential of  $V_{y1}$  and substituting (17), (18) and (20) into it, we can obtain

$$\dot{V}_{\theta 1} = z_1 z_2 - c_{\theta 1} z_1^2 \quad (21)$$

Taking the differential of  $Z_2$  and substituting (1), (18), and (20) into it, we can derive

$$\begin{aligned} \dot{z}_2 &= \dot{\omega}_r - \dot{\alpha}_{\theta 1} \\ &= -\frac{B}{J}(z_2 + \alpha_{\theta 1}) + \frac{k_t}{J}(u + d) + c_{\theta 1} \dot{z}_1 - \ddot{\theta}_r^* \end{aligned} \quad (22)$$

To design the position controller including the abilities of tracking input command and rejecting external load disturbance, we add the

related terms of  $Z_2$  and  $\hat{d}$  into  $V_{y1}$  to obtain a new Lyapunov function as

$$V_{\theta 2} = V_{\theta 1} + \frac{1}{2} \left( z_2^2 + \frac{1}{\gamma_{\theta}} \tilde{d}^2 \right) \quad (23)$$

where  $d$  is the estimated error between the value  $d$  and its estimated value  $\hat{d}$ , and  $\gamma_{\theta}$  is a positive constant. Finally, by using (21)–(23), and taking the differential of  $V_{y2}$ , it is not difficult to derive

$$\begin{aligned} \dot{V}_{\theta 2} &= \dot{V}_{\theta 1} + z_2 \dot{z}_2 + \frac{1}{\gamma_{\theta}} \dot{\tilde{d}} \tilde{d} \\ &= -c_{\theta 1} z_1^2 + z_2 \left[ z_1 - \frac{B}{J}(z_2 + \alpha_{\theta 1}) + \frac{k_t}{J}(u + \hat{d}) \right. \\ &\quad \left. + c_{\theta 1} \dot{z}_1 - \ddot{\theta}_r^* \right] - \frac{1}{\gamma_{\theta}} \tilde{d} \left( \dot{\hat{d}} - \gamma_{\theta} \frac{k_t}{J} z_2 \right) \end{aligned} \quad (24)$$

According to (24), the control input  $u$  can be obtained as

$$u = \frac{J}{k_t} \left( -c_{\theta 2} z_2 - z_1 + \frac{B}{J} \alpha_{\theta 1} - \frac{k_t}{J} \hat{d} - c_{\theta 1} \dot{z}_1 + \ddot{\theta}_r^* \right) \quad (25)$$

where  $C_1$  is a positive constant. The derivative of the estimated value,  $\hat{d}$ , can be expressed as

$$\dot{\hat{d}} = \gamma_{\theta} \frac{k_t}{J} z_2 \quad (26)$$

Substituting (25) and (26) into (24),  $V_{y2}$  is found to be negative and can be expressed as

$$\dot{V}_{\theta 2} = -c_{\theta 1} z_1^2 - \left( c_{\theta 2} + \frac{B}{J} \right) z_2^2 \leq 0 \quad (27)$$

Figure 3 shows the block diagram of the proposed position control drive system. By using a similar method to that for the speed control system mentioned previously, one can derive

$$\lim_{t \rightarrow \infty} z_1(t) = 0 \quad \text{and} \quad \lim_{t \rightarrow \infty} z_2(t) = 0 \quad (28)$$

Generally speaking, the selection of the positive constants is similar for both speed and position controls. A large value of  $C_1$  and  $C_2$  can increase the transient response. On the other hand, a small value of  $C_1$  can reduce the convergence time of the estimator. The selection depends on the designer's experience. If the positive constants are beyond their limitations, oscillations occur.

### 3.4 PI Speed Controller Design

The closed-loop speed control system with a PI controller is easily obtained. The transfer function of the closed-loop system at an external load equal to zero is

$$\begin{aligned} \frac{\omega_r(s)}{\omega_r^*(s)} &= \frac{\frac{K_t K_{p1}}{J} s + \frac{K_t K_{I1}}{J}}{s^2 + \frac{K_t K_{p1} + B}{J} s + \frac{K_t K_{I1}}{J}} \\ &= \frac{\beta_1}{s + \alpha_1} + \frac{\beta_2}{s + \alpha_2} \end{aligned} \quad (29)$$

$$\begin{aligned} \alpha_1 &= -\left( \frac{K_t K_{p1} + B}{2J} \right) \\ &\quad + \frac{1}{2} \sqrt{\left( \frac{K_t K_{p1} + B}{J} \right)^2 - 4 \frac{K_t K_{I1}}{J}} \end{aligned} \quad (30)$$

$$\beta_1 = \frac{\frac{K_t K_{p1}}{J} \left[ -\frac{(K_t K_{p1} + B)}{2J} + \frac{1}{2} \sqrt{\left(\frac{K_t K_{p1} + B}{J}\right)^2 - 4 \frac{K_t K_{t1}}{J}} \right] - \frac{K_t K_{t1}}{J}}{\sqrt{\left(\frac{K_t K_{p1} + B}{J}\right)^2 - 4 \frac{K_t K_{t1}}{J}}} \quad (31)$$

$$\alpha_2 = \frac{K_t K_{p1} + B}{2J} - \frac{1}{2} \sqrt{\left(\frac{K_t K_{p1} + B}{J}\right)^2 - 4 \frac{K_t K_{t1}}{J}} \quad (32)$$

$$\beta_2 = \frac{\frac{K_t K_{p1}}{J} \left[ \frac{K_t K_{p1} + B}{2J} + \frac{1}{2} \sqrt{\left(\frac{K_t K_{p1} + B}{J}\right)^2 - 4 \frac{K_t K_{t1}}{J}} \right] + \frac{K_t K_{t1}}{J}}{\sqrt{\left(\frac{K_t K_{p1} + B}{J}\right)^2 - 4 \frac{K_t K_{t1}}{J}}} \quad (33)$$

On the other hand, when the external load  $T_L$  is added, the speed dip of the drive system is

$$\begin{aligned} \frac{\Delta(\omega_r(s))}{T_L(s)} &= \frac{-\frac{1}{J}s}{s^2 + \frac{K_t K_{p1} + B}{J}s + \frac{K_t K_{t1}}{J}} \\ &= \frac{-\beta_{d1}s}{(s + \alpha_1)(s + \alpha_2)} \end{aligned} \quad (34)$$

$$\frac{\beta_1}{\alpha_1} + \frac{\beta_2}{\alpha_2} = 1 \quad (35)$$

$$\frac{\beta_1}{\alpha_1} e^{-0.3\alpha_1} + \frac{\beta_2}{\alpha_2} e^{-0.3\alpha_2} = 0.1 \quad (36)$$

$$-\left[ \frac{\beta_1}{\alpha_1} e^{-\frac{\alpha_1}{\alpha_2 - \alpha_1} \ln\left(\frac{\alpha_2}{\alpha_1}\right)} + \frac{\beta_2}{\alpha_2} e^{-\frac{\alpha_2}{\alpha_2 - \alpha_1} \ln\left(\frac{\alpha_2}{\alpha_1}\right)} \right] < 0.15 \quad (37)$$

$$\frac{\beta_{d1}}{\alpha_2 - \alpha_1} \left[ e^{-\frac{\alpha_1}{\alpha_2 - \alpha_1} \ln\left(\frac{\alpha_2}{\alpha_1}\right)} - e^{-\frac{\alpha_2}{\alpha_2 - \alpha_1} \ln\left(\frac{\alpha_2}{\alpha_1}\right)} \right] < 108 \quad (38)$$

Substituting (30)-(33) into (25)-(38), one can obtain:

$$0.19 < K_{p1} < 0.25 \quad (39)$$

and

$$0.26 < K_{t1} < 0.42 \quad (40)$$

In this paper, we select the parameters of the speed-loop controller as  $K_{p1} = 0.2$  and  $K_{t1} = 0.3$ .

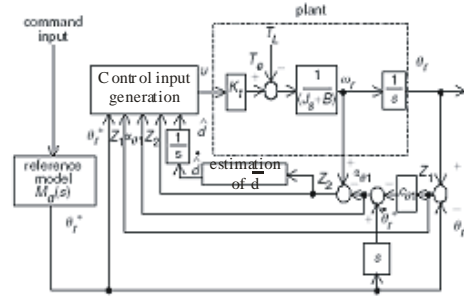


**Fig. 3** Block diagram of proposed position-control drive system

### 3.5 PI Position Controller Design

The transfer function of the closed-loop position system at

$$\frac{\theta_r(s)}{\theta_r^*(s)} = \frac{\frac{K_t K_{p2}}{J} s + \frac{K_t K_{t2}}{J}}{s^3 + \frac{K_t + B}{J} s^2 + \frac{K_t K_{p2}}{J} s + \frac{K_t K_{t2}}{J}} \quad (41)$$

After suitably reducing the order, the transfer function of the closed-loop position control system can be approximated to

$$\begin{aligned} \frac{\theta_r(s)}{\theta_r^*(s)} &\approx \frac{\frac{K_t K_{p2}}{J} s + \frac{K_t K_{t2}}{J}}{\sqrt{(K_t + B)^2 - 2K_t K_{p2} J} \sqrt{(K_t + B)^2 - 2K_t K_{p2} J}} \\ &\left( s^2 + \sqrt{\frac{K_t^2 K_{p2}^2 - 2K_t K_{t2} [(K_t + B) - \sqrt{(K_t + B)^2 - 2K_t K_{p2} J}]}{(K_t + B)^2 - 2K_t K_{p2} J}} s \right. \\ &\quad \left. + \frac{K_t K_{t2}}{\sqrt{(K_t + B)^2 - 2K_t K_{p2} J}} \right) \\ &= \frac{d_1 s + d_0}{s^2 + c_1 s + c_0} \end{aligned} \quad (42)$$

Where

$$c_1 = \sqrt{\frac{K_t^2 K_{p2}^2 - 2K_t K_{t2} [(K_t + B) - \sqrt{(K_t + B)^2 - 2K_t K_{p2} J}]}{(K_t + B)^2 - 2K_t K_{p2} J}}$$

$$c_0 = \frac{K_t K_{t2}}{\sqrt{(K_t + B)^2 - 2K_t K_{p2} J}} \quad (43)$$

$$d_1 = \frac{K_t K_{p2}}{\sqrt{(K_t + B)^2 - 2K_t K_{p2} J}} \quad (44)$$

(45)



$$d_0 = \frac{K_t K_{I2}}{\sqrt{(K_t + B)^2 - 2K_t K_{p2} J}} \quad (46)$$

Then, it is possible to rearrange (42) into two parts as follows:

$$\frac{\theta_r(s)}{\theta_r^*(s)} = \frac{\sigma_1}{s + \gamma_1} + \frac{\sigma_2}{s + \gamma_2} \quad (47)$$

$$\gamma_1 = \frac{-c_1 + \sqrt{c_1^2 - 4c_0}}{2} \quad (48)$$

$$\gamma_2 = \frac{-c_1 - \sqrt{c_1^2 - 4c_0}}{2} \quad (49)$$

$$\sigma_1 = \frac{d_1 \gamma_1 - d_0}{\gamma_1 - \gamma_2} \quad (50)$$

$$\sigma_2 = \frac{-(d_1 \gamma_2 - d_0)}{\gamma_1 - \gamma_2} \quad (51)$$

On the other hand, the transfer function between the position dip and the external load is

$$\frac{\Delta\theta_r(s)}{T_L(s)} = -\frac{\frac{1}{J}s}{s^3 + \frac{K_t + B}{J}s^2 + \frac{K_t K_{p2}}{J}s + \frac{K_t K_{I2}}{J}} \quad (52)$$

After suitably reducing the order of (52), one can obtain

$$\begin{aligned} \frac{\Delta\theta_r(s)}{T_L(s)} &\cong \frac{1}{\left( s^2 + \sqrt{\frac{K_t^2 K_{p2}^2 - 2K_t K_{I2} [(K_t + B) - \sqrt{(K_t + B)^2 - 2K_t K_{p2} J}]}{(K_t + B)^2 - 2K_t K_{p2} J}} + \frac{K_t K_{I2}}{\sqrt{(K_t + B)^2 - 2K_t K_{p2} J}} \right)} \\ &= -\frac{\beta_{d2} s}{(s + \gamma_1)(s + \gamma_2)} \end{aligned} \quad (53)$$

and

$$\beta_{d2} = \frac{1}{\sqrt{(K_t + B)^2 - 2K_t K_{p2} J}} \quad (54)$$

The specification of the position control system is shown as follows. The steady-state position error  $e_{ss} = 0$ , the risetime  $t_r = 0.15s$ , the maximum overshoot  $M_p 15\%$ , the maximum position dip at an external load  $0.7.8\%$ . Then, according to the required specification, one can derive the following:

$$\frac{\sigma_1}{\gamma_1} + \frac{\sigma_2}{\gamma_2} = 1 \quad (55)$$

$$\frac{\sigma_1}{\gamma_1} e^{-0.15\gamma_1} + \frac{\sigma_2}{\gamma_2} e^{-0.15\gamma_2} = 0.1 \quad (56)$$

$$-\left[ \frac{\sigma_1}{\gamma_1} e^{-\frac{\gamma_1}{\gamma_2 - \gamma_1} \ln\left(\frac{\sigma_2}{\sigma_1}\right)} + \frac{\sigma_2}{\gamma_2} e^{-\frac{\gamma_2}{\gamma_2 - \gamma_1} \ln\left(\frac{\sigma_2}{\sigma_1}\right)} \right] < 0.15 \quad (57)$$

$$\frac{\beta_{d2}}{\gamma_2 - \gamma_1} \left[ e^{-\frac{\gamma_1}{\gamma_2 - \gamma_1} \ln\left(\frac{\gamma_2}{\gamma_1}\right)} - e^{-\frac{\gamma_2}{\gamma_2 - \gamma_1} \ln\left(\frac{\gamma_2}{\gamma_1}\right)} \right] < 14 \quad (58)$$

Substituting (48)–(51) into (55)–(58), one can derive

$$9.5 < K_{p2} < 13.2 \quad (59)$$

and

$$17.3 < K_{I2} < 24.8 \quad (60)$$

In this paper, we select the position controller as  $K_{p2} = 10$  and  $K_{I2} = 20$ . The relationship between PI speed controller and PI position controller cannot be derived because the speed control system and the position control system have different specifications.

Regarding the controller design, a good transient response is required for the IM drive system. In addition, the load disturbance response should perform a low dip and a small value of the integral square error (ISE). By using the proposed adaptive backstepping controller, the specification of the risetime for speed controller and position controller are set as 0.2 and 0.15s, respectively. Therefore, the reference model in Figs. 2 and 3 can be derived as  $M_d(s) = 167.96/(s^2 + 25.92s + 167.96)$  and  $M_d(s) = 672.36/(s^2 + 51.86s + 672.36)$  individually. As for the PI controller design, in order to decide the parameters of  $K_p$  and  $K_I$ , the specifications of the drive system are required. For example, the risetime of the transient response, the maximum overshoot and the maximum dip of the external load disturbance should be clearly determined. For a fair comparison, the risetime of the speed drive is set as 0.3s and the risetime of the position



control system is set as 0.15s. In this paper, to simplify the design procedures,  $K_p$  is determined first. Then,  $K_I$  is carefully chosen. By decreasing the value of  $K_I$ , the overshoot of the transient response can be reduced. However, reducing  $K_I$  could cause a large speed dip or a position dip when the external load is added. The opposite results are obtain when  $K_I$  is increased. In this paper, the PI controller is selected according to the trade-off among the maximum overshoot, dip and ISE.

The transient responses and load disturbance dips are shown in Tables 1 and 2 when  $K_I$  parameter is varied. As one can observe, when we select a small value of  $K_I$ , the maximum overshoot can be as good as the adaptive backstepping controller. However, when the external load is added, the load disturbance rejection capability obviously deteriorates. On the other hand, by selecting a large  $K_I$  parameter, the maximum dip can be obviously improved; unfortunately, the overshoot of the transient response is abruptly increased. From Tables 1 and 2, one can conclude that it is impossible to achieve both a good transient response and a good load disturbance response by using only a PI controller.

Table 1: Results of varying  $K_I$  for speed-control system

Table 1: Results of varying  $K_I$  for speed-control system

$K_p$	$K_I$	Percentage of maximum overshoot	Percentage of maximum dip	ISE value on load disturbance
0.2	0.075	2.32%	8.28%	27497
0.2	0.15	6.02%	7.74%	13830
0.2	0.3	11.56%	7.02%	6921.6
0.2	0.6	19.14%	6.17%	3465.8
0.2	1.2	28.59%	5.24%	1738.0

Table 2: Results of varying  $K_I$  for position control system

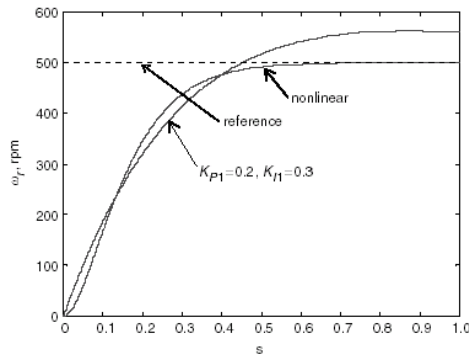
$K_p$	$K_I$	Percentage of maximum overshoot	Percentage of maximum dip	ISE value on load disturbance
10	5	4.22%	8.76%	307.5802
10	10	7.53%	8.29%	155.4748
10	20	12.84%	7.65%	78.5078
10	40	20.79%	6.88%	40.0448
10	80	31.94%	6.01%	20.8630

The adaptive backstepping controller tunes its parameters according to the operating environment. As a result, it can achieve both a good transient response and a good load

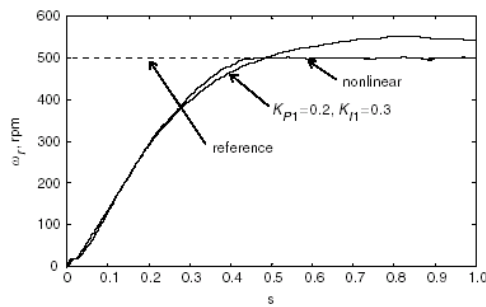
disturbance response. Moreover, from experimental results, the adaptive backstepping controller performs better when the controller tracks a time-varying command, such as a sinusoidal command or a triangular command. The major reason is that a PI controller may cause serious steady-state error and phase-lag problem. As we know, a PI controller can track a step input but cannot track a time varying command well owing to its phase-lag problem. The details of the experimental results will be shown and discussed in Section 4. It is possible to choose new parameters of the PI controller and the adaptive backstepping controller for the drive system carefully to reduce the risetime. According to the experimental results, for the best case, the risetime of the speed controller and position controller can be set as 0.13 and 0.1 s, respectively. The results are also shown in Section 4. According to the experimental results, the performance of the adaptive backstepping controller is again better than that of the PI controller.

#### 4 Experimental results

In the work described in this paper, the digital signal processor TMS320C40 serves as the controller. The input voltage source of the matrix converter is three-phase, 220 V, 60 Hz. The parameters of the IM are:  $R = 0.12 / \text{phase}$ ,  $L_d = L_q = 6.8\text{mH}$ ,  $J = 0.0063 \text{ Nms}^2 / \text{rad}$ ,  $B = 0.0015 \text{ Nms/rad}$ ,  $K_t = 0.653 \text{ Nm/A}$ . The sampling time of the current-loop is 100ms and the sampling time of the speed or position loop is 1 ms. Several experimental results are shown here. The parameters of the PI controller are selected according to the detailed analysis mentioned in Section 3. The selection of the parameters of the PI controller is determined by the specifications of transient response, overshoot and load disturbance response. Figures 4a and b show the transient speed responses of a 500 rpm step-input speed command without an external load. Figures 5a and b show the load disturbance speed responses at 500rpm when an external load of 2Nm is added. As can be seen, the nonlinear controller has a better performance than the PI controller. Figure 6 shows the measured lowspeed response at 15 rpm without an external load. Figure 7 shows the measured speed response at a rated speed of 1500rpm without an external load. Figures 8a–c show some measured speed-tracking responses.

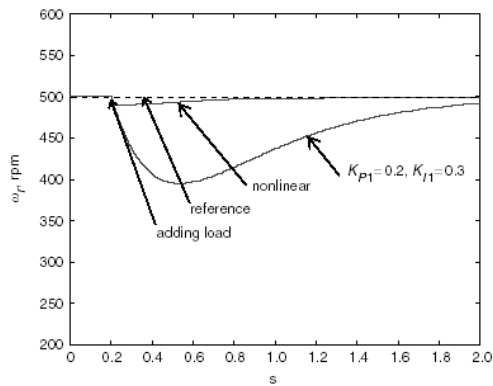


(a)

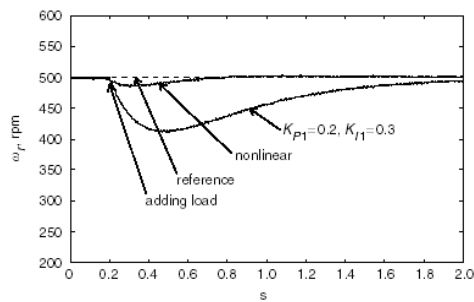


(b)

**Fig. 4** Transient speed responses



(a)



(b)

**Fig. 5** Speed-load disturbance responses

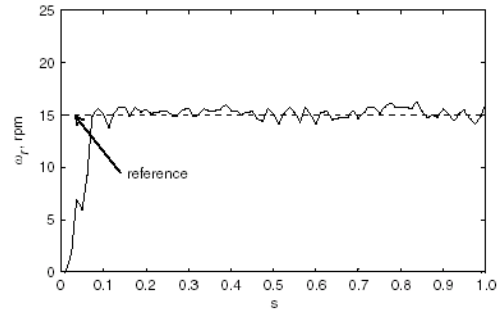


**Fig. 6** Measured low-speed response at 15 rpm

Figure 8a is the tracking response of a square-wave command. Figure 8b is the tracking response of a sinusoidal command. Figure 8c is the tracking response of a triangular command. As can be seen, the proposed adaptive backstepping controller can track a time-varying speed command better than the PI controller. Figure 9 shows the measured speed responses for different inertia without an external load. Although the inertia is varied more than three times, the proposed controller has similar speed responses. Figures 10a and b show the transient position responses without an external load. Figures 11a and b show the position response when an external load of 2Nm is added. Again, the

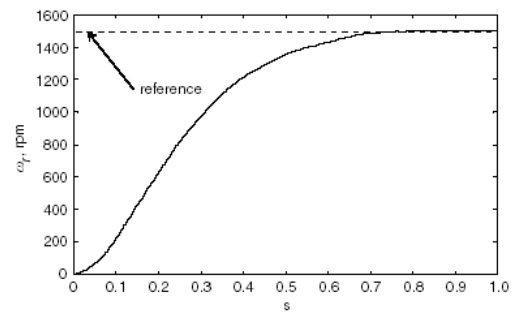
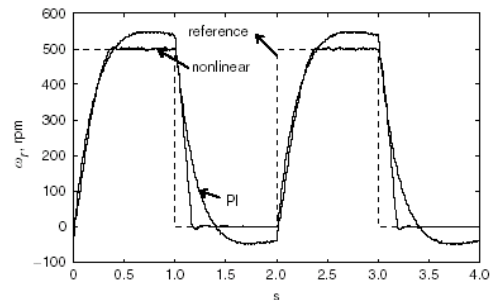
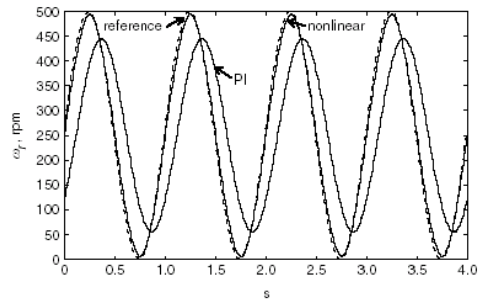


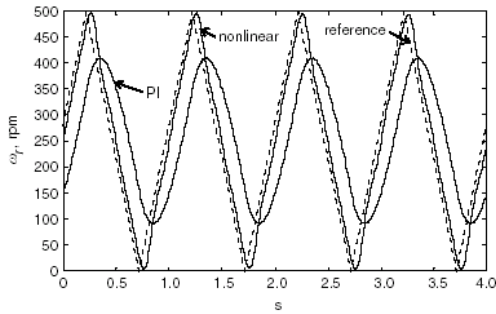
**Fig. 7** Measured speed response at 1500 rpm



(a)



(b)



(c)

Fig. 8 Measured speed-tracking responses

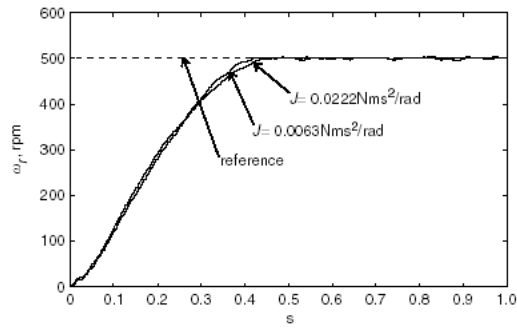
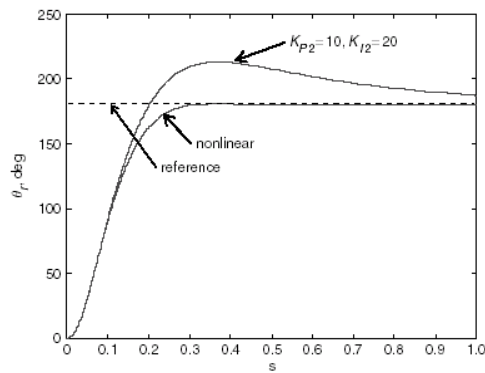
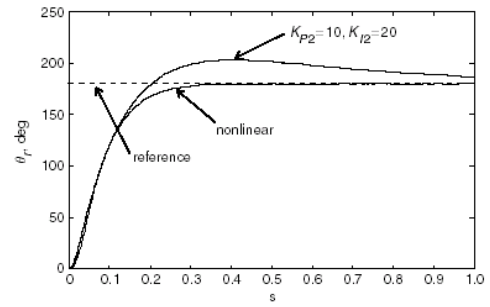


Fig. 9 Measured speed responses for different inertia

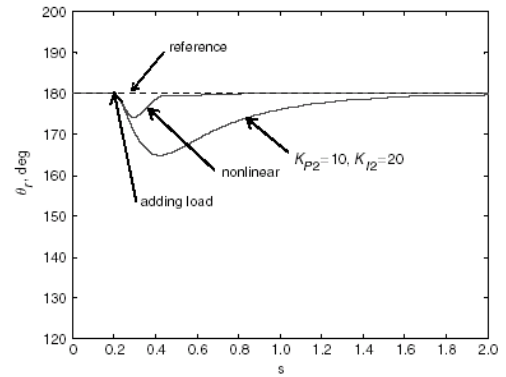


(a)

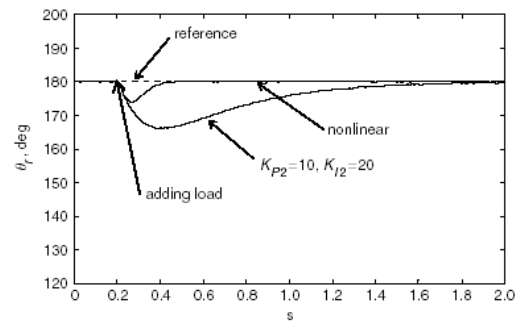


(b)

Fig. 10 Transient position responses

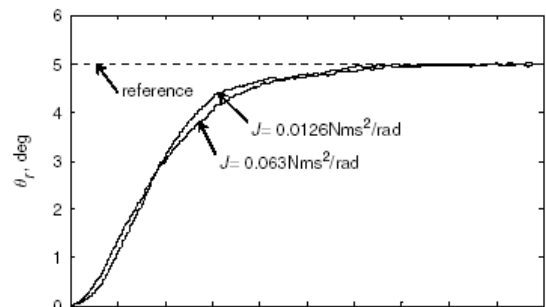


(a)

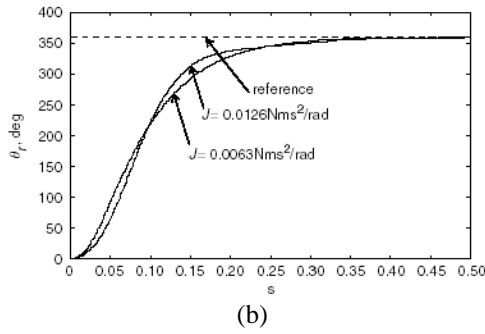


(b)

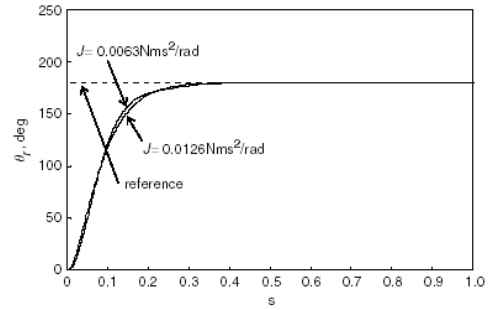
Fig. 11 Position load disturbance responses (a) Simulated (b) Measured



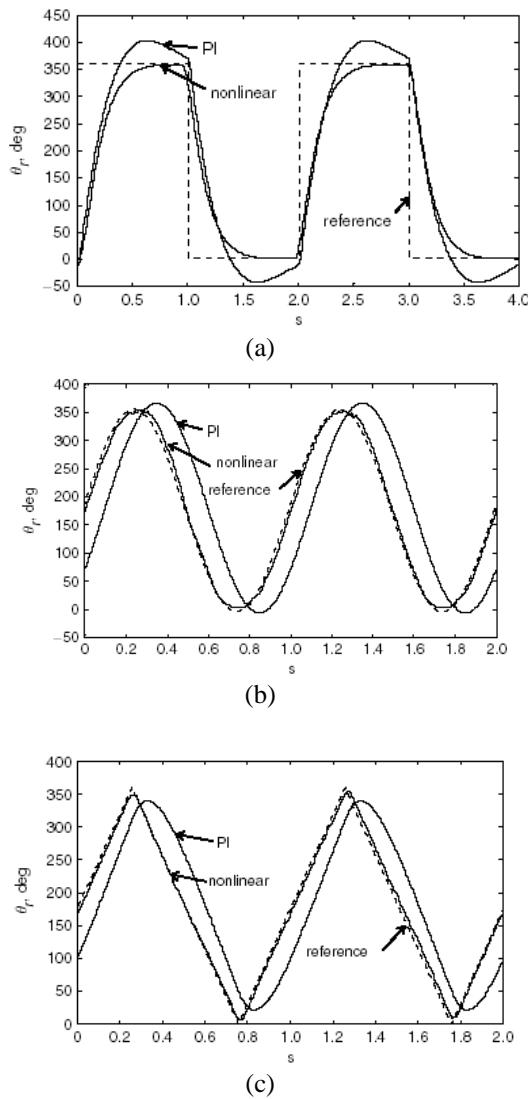
(a)



**Fig. 12** Measured position responses of different inertia (a) 5 mechanical degrees (b) 360 mechanical degrees

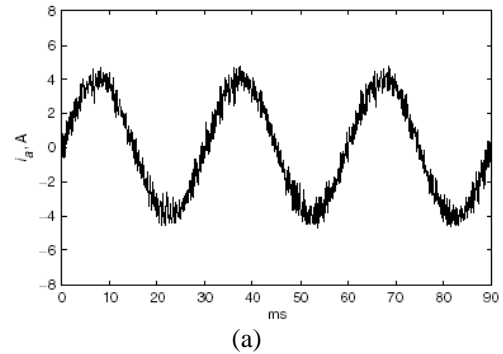


**Fig. 14** Measured position responses for different inertia



**Fig. 13** Measured position-tracking responses (a) Square wave, (b) Sinusoidal, (c) Triangular

nonlinear controller has better responses than the PI controller. Figure 12a is the measured small-angle position responses for different inertia without an external load. The responses of a 5 mechanical degree rotation are shown here. Figure 12b shows the measured large-angle position responses of different inertia. It is a 360 mechanical degree rotation without an external load. Figures 13a–c show the measured position-tracking responses, which include a square-wave, a sinusoid and a triangular command. Again, the measured results show the proposed system has a satisfactory tracking ability. Figure 14 shows the measured position responses for different inertia. The inertia is varied by coupling a DC motor to increase total inertia. The results show that the system is very robust. Figures 15a–c show the measured steady state waveforms of matrix converter. Figure 15c shows the measured input A-phase current of the matrix converter. According to Fig. 15c, the fundamental component is a sinusoidal current. Figures 16a and b show the responses when the stator resistance of the motor varies in a wide range. Figure 16a is the speed response. Figure 16b is the position response.



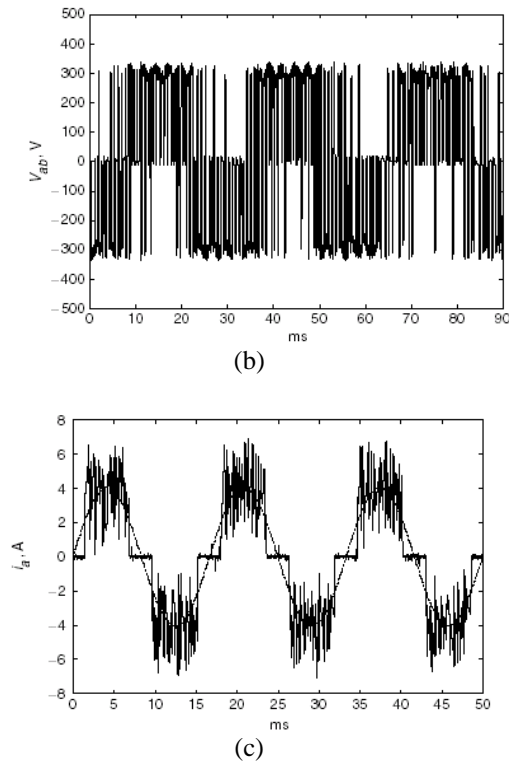


**Fig. 15** Measured steady-state waveforms of matrix converter (a) Output current, (b) Output voltage, (c) Input current

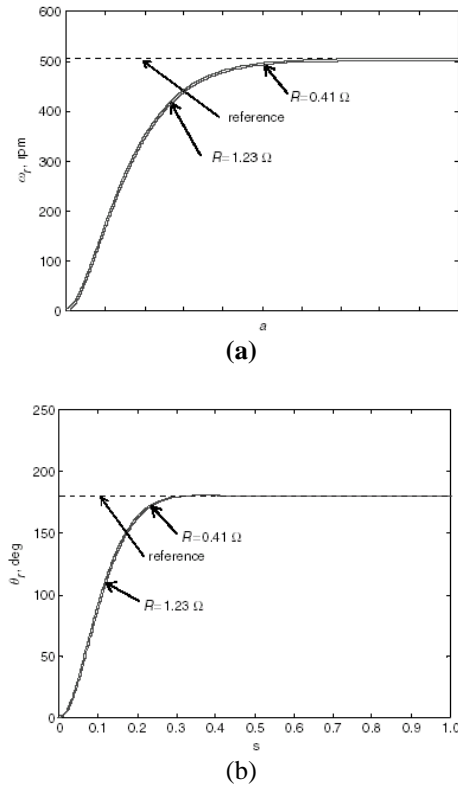


**Fig. 16** Responses for different stator resistances (a) Speed, (b) Position

The proposed adaptive backstepping controller performs better than the PI controller. There are several reasons for this. For example, by using the backstepping controller, the external load can be online estimated and suitably compensated by the control input both in speed control and position control. In, the converge rate of the speed error or position error can be determined by the designer. The PI controllers from Fig. 4 to Fig. 13 are obtained by the specification mentioned in Section 3. It is possible that the PI control design assumptions are not justified owing to the specification mentioned in Section 3. These assumptions can drive the slow response of the PI control loop and hence result in poor performance. To improve this situation, Figs. 17 and 18 show the results from using new parameters of the PI controller and the backstepping controller. The most important purpose is to drive the system as fast as possible. Figures 17a and b show the measured speed responses. By suitably adjusting parameters, the PI controller can have a similar transient response to that of the adaptive backstepping controller; however, the PI controller has a worse load disturbance response than the adaptive backstepping controller when an external load is added.

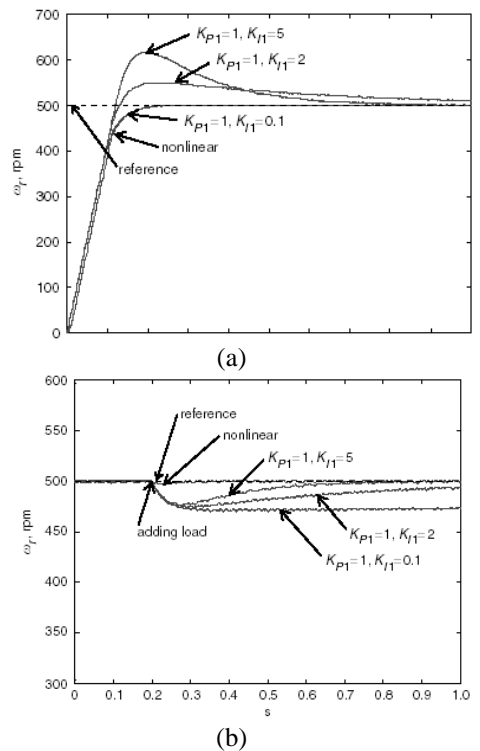


**Fig. 17.** Improved speed responses (a) Transient (b) load disturbance

The major reason is that the PI controller cannot achieve both a fast transient response and a good load disturbance response. It is well known that integration term, KI, can be improved to reduce the steady-state error, but it causes overshoot in transient response as well. Figures 18a and b show the measured position responses of the PI controller and adaptive backstepping controller.

As can be seen, by suitably adjusting the parameters, the PI controller has a similar response to that of the adaptive backstepping controller. However, when a 2Nm load is added, the PI controller performs a more serious position disturbance than the adaptive backstepping controller. The load disturbance response of the PI controller can be improved by increasing the parameter  $K_I$ ; unfortunately, its related transient response has an obvious overshoot as the parameter  $K_I$  is increased. From the experimental results, we can conclude that the backstepping controller is better than the PI controller for the proposed matrix-converter IM drive system.

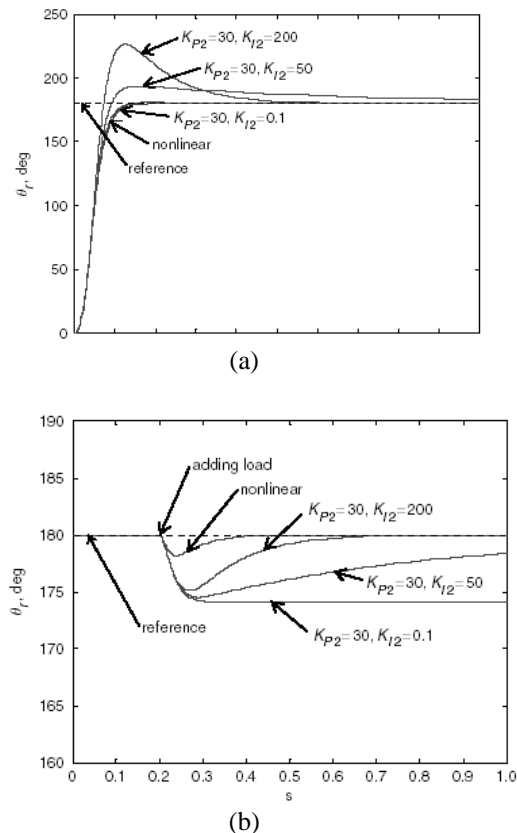


**Fig. 18** Improved position responses (a) Transient (b) Load disturbance

## 5 CONCLUSIONS

The design and implementation of a novel controller design for a matrix converter-based IM system have been investigated. All the control algorithms, which include the switching strategy, the co-ordinate transformation, the speed control, and the position control, are executed by a digital signal processor. This paper provides a systematic and analytic method for designing a high performance matrix-converter-based IM system. The proposed design approach has been validated by actual implementation. As a result, a new direction is provided for matrix converter-drive systems.

The impact of these results on the future work in IM control is in speeding-up process of the matrix converter technology in real industrial applications. As a result, it is likely to play major role in future converter designs both as a motor drive at low and high powers and as a power converter linking two electrical power systems having different voltages and frequencies.

## 7. REFERENCES

- 1 Wheeler, P.W., Rodriguez, J., Chars, J.C., Empringham, L., and Weinstein, A.: 'Matrix converters: a technology review', *IEEE Trans. Ind. Electron.*, 2002, 49, (2), pp. 276–288.
- 2 Klumpner, C., Nielsen, P., Boldea, I., and Blaabjerg, F.: 'New solutions for a low-cost power electronic building block for matrix converters', *IEEE Trans. Ind. Electron.*, 2002, 49, (2), pp. 336–342.
- 3 Kim, S., Sul, S.K., and Lipo, T.A.: 'AC/AC power conversion based on matrix converter topology with unidirectional switches', *IEEE Trans. Ind. Appl.*, 2000, 36, (1), pp. 139–145.
- 4 Casadei, D., Serra, G., and Tani, A.: 'The use of matrix converters in direct torque control of induction machines', *IEEE Trans. Ind. Electron.*, 2001, 48, (6), pp. 1057–1064.
- 5 Casadei, D., Serra, G., Tani, A., and Zarri, L.: 'Matrix converter modulation strategies: a new general approach based on space-vector representation of the switch state', *IEEE Trans. Ind. Electron.*, 2002, 49, (2), pp. 370–381.



- 6 Milanovic, M., and Dobaj, B.: 'Unity input displacement factor correction principle for direct AC to AC matrix converters based on modulation strategy', *IEEE Trans. Circuits Syst. I*, 2000, 47, (2), pp. 221–230.
- 7 Helle, L., Larsen, K.B., Jorgensen, A.H., Stig, M.N., and Blaabjerg, F.: 'Evaluation of modulation schemes for three-phase to three-phase matrix converters', *IEEE Trans. Ind. Electron.*, 2004, 51, (1), pp. 158–171.
- 8 Nielsen, P., Blaabjerg, F., and Pedersen, J.K.: 'New protection issues of a matrix converter: design considerations for adjustable-speed drives', *IEEE Trans. Ind. Appl.*, 1999, 35, (5), pp. 1150–1161.
- 9 Liaw, C.M., and Cheng, S.Y.: 'Fuzzy two-degree-of-freedom speed controller for motor drives', *IEEE Trans. Ind. Electron.*, 1995, 42, (2), pp. 209–216.
- 10 Liu, T.H., Chen, S.H., and Chen, D.F.: 'Design and implementation of a matrix converter IM drive without a shaft sensor', *IEEE Trans. Aerosp. Electron. Syst.*, 2003, 39, (1), pp. 228–243.
- 11 Klumpner, C., Nielsen, P., Boldea, I., and Blaabjerg, F.: 'A new matrix converter motor (MCM) for industry applications', *IEEE Trans. Ind. Electron.*, 2002, 49, (2), pp. 325–335.
- 12 Antoni Arias, Cesar A. Silva, Greg M. Asher, Jon C. Clare and Patrick W. Wheeler "Use of matrix converter to enhance the sensorless control of a surface mount permanent magnet AC motor at zero and low frequency," *IEEE Trans. Ind. Electron.*, vol. 53, no. 2, pp. 440-449, April 2006.
- 13 Meharegzi Tewelde and Shyam P. Das "A novel control of bidirectional switches in matrix converter," *proceedings of IEEE , PEDES*, December 12-15, New Delhi , India, , pp. 240-246, 2006